# Responsive and self-healing structural color supramolecular hydrogel patch for diabetic wound treatment

Canwen Chen [a],[1], Yu Wang [a],[b],[1], Han Zhang [b], Hui Zhang [b], Weiliang Dong [c],[*], Weijian Sun [d],[**], Yuanjin Zhao [a],[b],[***]

[a] *Department of Rheumatology and Immunology, Institute of Translational Medicine, The Affiliated Drum Tower Hospital of Nanjing University Medical School, Nanjing, 210008, China*
[b] *State Key Laboratory of Bioelectronics, School of Biological Science and Medical Engineering, Southeast University, Nanjing, 210096, China*
[c] *State Key Laboratory of Materials-Oriented Chemical Engineering, College of Biotechnology and Pharmaceutical Engineering, Nanjing Tech University, Nanjing, 211800, China*
[d] *Department of Gastrointestinal Surgery, The Second Affiliated Hospital of Wenzhou Medical University, Wenzhou, 325027, China*

## ARTICLE INFO

## ABSTRACT

The treatment of diabetic wounds remains a great challenge for medical community. Here, we present a novel structural color supramolecular hydrogel patch for diabetic wound treatment. This hydrogel patch was created by using N-acryloyl glycinamide (NAGA) and 1-vinyl-1,2,4-triazole (VTZ) mixed supramolecular hydrogel as the inverse opal scaffold, and temperature responsive poly(N-isopropylacrylamide) (PNIPAM) hydrogel loaded with vascular endothelial cell growth factor (VEGF) as a filler. Supramolecular hydrogel renders hydrogel patch with superior mechanical properties, in which NAGA and VTZ also provide self-healing and antibacterial properties, respectively. Besides, as the existence of PNIPAM, the hydrogel patch was endowed with thermal-responsiveness property, which could release actives in response to temperature stimulus. Given these excellent performances, we have demonstrated that the supramolecular hydrogel patch could significantly enhance the wound healing process in diabetes rats by downregulating the expression of inflammatory factors, promoting collagen deposition and angiogenesis. Attractively, due to responsive optical property of inverse opal scaffold, the hydrogel patch could display color-sensing behavior that was suitable for the wound monitoring and management as well as guidance of clinical treatment. These distinctive features indicate that the presented hydrogel patches have huge potential values in biomedical fields.

## 1. Introduction

Diabetes mellitus, a worldwide chronic disease, brings about a non-healing chronic wound that seriously endangers human health every year [1–8]. Owing to prolonged inflammatory period, reduced neo-vascularization, and impaired endothelial cell function, the healing process in diabetic wound is hampered [9–15]. Considerable efforts have been devoted to generating materials for the treatment of diabetic wound, such as rubber, nanofibers, porous foams, and hydrogel patches [16–23]. Among them, hydrogel patches show great potential in diabetic wound healing due to their deformability, moisture retention, as well as the advantages of internalizing and delivering actives at the wound interface [24–28]. Although with much progress, the existing hydrogel patches are usually with simple composition or structures, which would restrict their functional performance in responsiveness, antibacterial and anti-inflammatory capabilities. In addition, insufficient mechanical strength and brittle nature of hydrogel patches could make them inapplicable in the dynamic wounds with sustained

deformations. Moreover, most of the hydrogel patches are lacking of real-time monitoring property, which is essential for evaluating the wound conditions. Thus, the development of responsive, multifunctional hydrogel patches with good mechanical strength, self-healing capability, and self-reporting feature is still highly anticipated for efficient diabetic wound healing.

In this paper, we present a novel supramolecular hydrogel structural color patch with the desired features for the treatment of diabetic wound, as schemed in Fig. 1. Supramolecular hydrogels, derived from the assembly of supramolecular polymer networks, are fascinating materials similar to natural extracellular matrix (ECM) [29–33]. Benefiting from their excellent properties, including suitable mechanical strength, self-healing, antibacterial and anti-inflammatory, supramolecular hydrogels have found many applications in biomedical areas [34–37]. In contrast, structural colors, as a type of coloration arising from unique interaction of light with intrinsic periodic nanostructures, have aroused great attention in optical displays, anti-counterfeiting labels, wearable electronics, etc [38–40]. In particular, when the structural color materials were constructed by responsive polymers, their colors could be tuned by swelling or shrinking these polymers with different stimulations, which indicate the potential sensor values of these materials [41, 42]. Therefore, it is conceivable that the integration of supramolecular hydrogel with structural colors would provide a distinctive strategy for the construction of a novel hydrogel patch for diabetic wound treatment.

Herein, we created the responsive and self-healing structural color supramolecular hydrogel patch by employing NAGA and VTZ mixed polymers as the inverse opal scaffold, and temperature responsive PNIPAM hydrogel as a filler. Due to the hydrogen bonds and the non-covalent interaction reversibility of NAGA network, the resultant (NAGA-VTZ) & PNIPAM hydrogel (NNH) patch could not only show superior mechanical performance, but also have self-healing capability. This hydrogel patch was also imparted with good antibacterial bioactivities because of the presence of VTZ. In addition, taking advantage

of thermal-responsiveness performance of the PNIPAM polymer, the hydrogel patch could release the actives when applied to the wound site with relatively high temperature caused by inflammation. Based on these advantages, we have demonstrated that the proposed structural color supramolecular hydrogel patches could significantly enhance the wound healing process in diabetes rats by downregulating the expression of inflammatory factors, and promoting collagen deposition and angiogenesis. Notably, benefit from the unique optical property of inverse opal scaffold, the hydrogel patch could even exhibit color-changing ability in response to temperature stimuli, which showed great potential in wound monitoring and management as well as guidance of clinical treatment.

## 2. Experimental section

***Materials:*** Monodispersed silica nanoparticles were obtained by Yuanjin Zhao's group. N-Acryloyl glycinamide (NAGA), 1-vinyl-1,2,4-triazole (VTZ), 2-hydroxy-4'-(2hydroxyethoxy)-2-methyl-propiophenone (2959), N, N′-methylenebis(acrylamide) (BIS) and N-isopropylacrylamide (NIPAM), were purchased from Sigma-Aldrich (USA). The Live & Dead Viability/Cytotoxicity Assay Kit, and MTT Cell Proliferation and Cytotoxicity Assay Kit (MTT) were purchased from KeyGen Biotech Co.,Ltd. (Nanjing, China). The male Sprague−Dawley rats (8-week-old) were bought from Reagan Biotechnology Co. (Shanghai, China). All operations were performed following the Laboratory Animal Care and Use Guidelines (NIH Publication no. 80-23 Rev. 1978). And these operations were approved and authorized by the Comparative Medicine Division of Jinling Hospital.

***Preparation of silica colloidal crystal templates*** (***SCCs***)**:** The SCCs were prepared as previously described.[39] Ultrasonically cleaned and oxygen plasma-treated slides were immersed in a solution of monodisperse silica nanoparticles at a concentration of 5%. SCCs with distinct structural colors were obtained after self-assembly by evaporation at
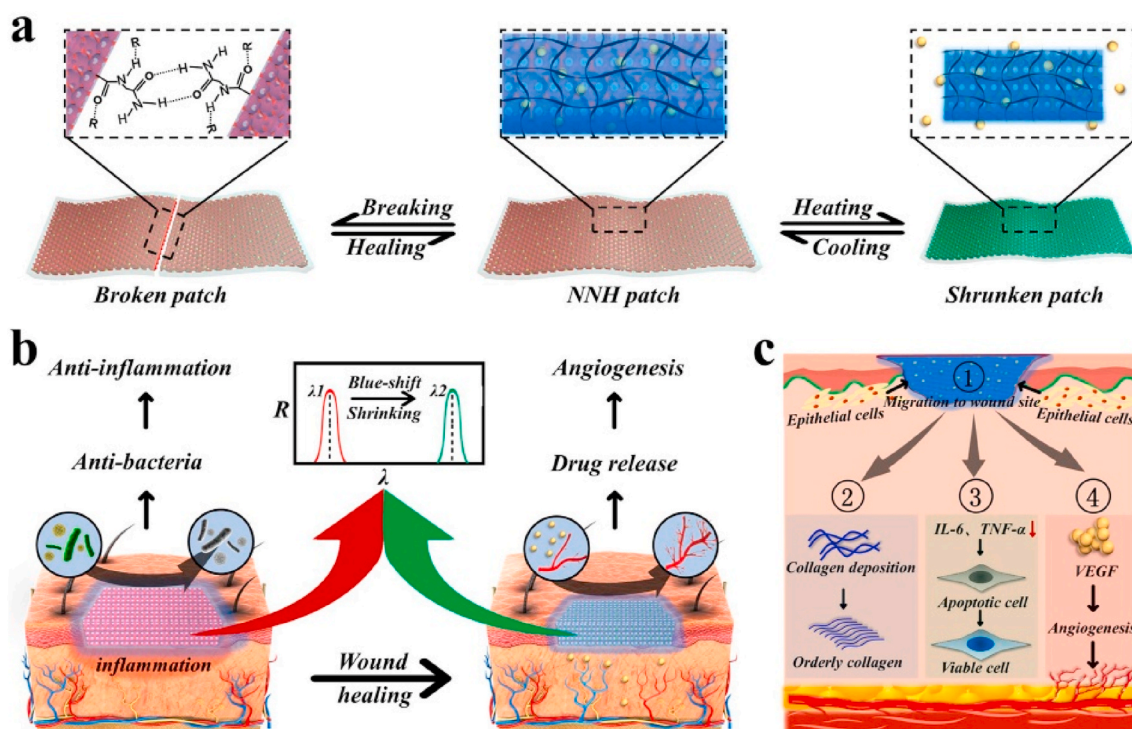


**Fig. 1.** Schematic representation of the excellent performance of the NNH patches and their application to diabetic wound. a) The self-healing and temperature-responsive performances of NNH patches, b) The patches for treatment of diabetic wound. c) Schematic illustration of the mechanism of NNH patch in promoting diabetic wound healing: 1) NNH facilitated the migration of epithelial cells by created moist environment. 2) The patch improved the undesirable collagen deposition. 3) The patch controlled wound infection by down-regulating inflammatory factors and 4) promoted the reconstruction of the blood vessels and microcirculation by delivering VEGF to wounds.

60 °C for 2 d under ventilated conditions.

***Fabrication of bioinspired multifunctional NNH patches:*** Firstly, the PNAGZ (polymer of NAGA and VTZ) inverse opal scaffolds were negatively replicated from the voids of the SCCs. The prepared SCCs were soaked in PNAGZ pregel solution (20% (w/v) NAGA monomer, 0.6‰ (v/v) VTZ monomer, and 5‰ (v/v) 2959) for 5 min. After that, the pregel solution was cured by UV light. Subsequently, the hybrid films were immersed in hydrofluoric acid (4%, v/v) to etch the SCCs. After 24 h, the PNAGZ inverse opal scaffolds were obtained after repeatedly rinsing with pure water more than 10 times. Then, the PNAGZ inverse opal scaffolds were placed in molds containing different concentrations of PNIPAM pre-gel solutions (5% (w/v) to 20% (w/v) NIPAM monomer, BIS (ten percent of NIPAM), and 5‰ (v/v) 2959). The mold was placed in a vacuum environment. After 30 min, the mold was exposed to UV light for a few seconds, curing the NIPAM monomer. Finally, the bioinspired multifunctional structural color hydrogel patches were prepared. In addition, various NNH patches can be obtained by using PNAGZ inverse opal scaffolds with different reflection peaks.

***Self-Healing Effect of NNH patches:*** The different NNH patches were cut into rectangles of similar size. The separate NNH patches were baselined together, and tightly connected to each other. Then, these patches were placed in a sealed mold and held at 40 °C for 90 min. Finally, the patches were demolded, and formed a healed three-dimensional rectangular body. Furtherly, the compression tests were employed to confirm their self-healing efficiency.

***Temperature stimulus responsiveness of NNH patches:*** The NNH patches were set at 37 °C to observe and record their shrinkage state while detecting the changes of the reflection peaks. When the contraction stopped, the patches were then placed at room temperature to swell fully. This process was repeated to examine the fatigue resistance of NNH patches in response to stimulation of volume phase transition temperature (VPTT), and the ratio of contractions of different patches in response to stimulation of VPTT. For the temperature-dependent release experiments, different concentrations of PNIPAM pre-gel solutions were firstly mixed with FITC-BSA. Then the generated patches were placed at surroundings of 37 °C, 1 atm (simulating a microenvironment of chronic diabetic wounds) and at surroundings of 25 °C, 1 atm, respectively, to achieve a drug release profile. The supernatant was taken 1 mL at each scheduled time point and then replaced with an equal amount of fresh buffer solution. Then, the Microplate Reader was employed to examine the release of the FITC-BSA. Finally, the results were further quantified according to the standard calibration curves of FITC-BSA. Six parallel samples were set up in this experiment.

***In vitro Antibacterial Tests:*** Antibacterial tests were performed by using the previous procedure [43]. *S. aureus* and *E. coli* strains were used to examine the antibacterial activity of NNH patches. Firstly, *Staphylococcus aureus* or *Escherichia coli* suspensions with a turbidity of approximately 0.5 were prepared according to the MacFarlane standard. The bacterial suspensions were subsequently treated with NNH patches prepared from pure water as a solvent for various reagent monomers and NNH patches prepared from MES buffer at pH 6.0 as a solvent for various reagent monomers, respectively. The non-treated group served as a blank control. After 24 h, live-dead staining results were recorded by confocal microscopy, while bacterial morphology was observed by SEM.

***Cell compatibility assessment:*** The experiments were performed as previously described [44,45]. Before culture with cells, the NNH patches were treated successively by dialysis of PBS, sterilization of ethanol and UV disinfection. The L929 cells were cultured in complete DMEM under the surrounding of 5% $CO_2$ at 37 °C. Cells at a concentration of $2 \times 10^5$ live cells/mL were then transferred to 24-well plates with or without NNH patches. Then 0.5 mL of complete DMEM was added to each well. The cultured cells were classified into three groups: blank control (cultured in blank wells), NNH group (NNH patches prepared using pure water as solvent) and NNH (MES) group (NNH patches prepared using MES buffer as solvent). Three parallel controls were set up for each group. After culturing for 24 h, cell viability was detected by the MTT assay.

***Preparation of diabetic model in rats:*** Diabetic wound healing model was established as previously described [46]. After 16 h of fasting, all rats were injected intraperitoneally with streptozotocin (STZ) (60 mg/kg) to diabetic mellitus. After 72 h, all rats showed symptoms of polyphagia, polydipsia, and polyuria. The blood glucose level of the rats was measured, and the diagnosis of diabetes was confirmed with blood glucose above 300 mg/dL. Then, a circular full-thickness wounds of 7 mm in diameter on the back of the rat was removed by hole puncher. Diabetic rats were randomly classified into five groups: blank group (wound treated with PBS), CSD group, VEGF group (injected in the wound with 100 μl of 1ug/ml VEGF), NNH patches group and NNH-VEGF patches group. Six parallel samples were set up in each group. The images of wounds were recorded at 0, 1, 5 and 10 days after operation. The rats were sacrificed after 10 days, and the granulation tissue was excised. The granulation tissues were immediately preserved by immersion in 4% paraformaldehyde for next histological examination, immunohistochemical detection, and immunofluorescence staining. The granulation tissues for quantitative real-time PCR (qPCR) were stored at −80 °C.

***In vivo diabetic wound healing:*** The obtained granulation tissues were embedded in paraffin wax. The wax blocks were then sectioned through a microtome. Masson trichrome staining, H&E staining, immunohistochemistry and immunofluorescence staining were performed separately for each group of sections. Immunohistochemical sections were used to observe the presence of pro-inflammatory factors interleukin-6 (IL-6) and tumor necrosis factor-α (TNF-α). Immunofluorescence staining was used to observe the expression of CD31 and α-SMA. QPCR analysis was used to detect the mRNA expression of TNF and IL-6. The experiments were supported by the experimental technician of Wuhan Google Biotechnology Co., Ltd.

## 3. Results and discussion

In a typical experiment, monodisperse silica nanoparticles were self-assembled by solvent evaporation and created tightly aligned arrays to obtain SCCs for the subsequent production of multifunctional structural color hydrogel patches, as shown in Fig. 2a. Secondly, the pregel solution of NAGA and VTZ was fully penetrated into nanogaps of SCCs because of capillary action, and then a hybrid film of SCCs and PNAGZ hydrogel was formed by ultraviolet (UV) photopolymerization (Fig. 2aii, 2c). Subsequently, the hydrogel inverse opal scaffolds with periodic porous structures were got by etching SCCs. Last, after filling and curing of thermal-responsive PNIPAM hydrogels into the nanogaps of inverse opal scaffolds, the free-standing NNH patch was obtained (Fig. 2aiv, 2d). Benefiting from the strong cross-linking network of PNAGZ hydrogel, the NNH patches could show great mechanical properties. Supporting this, it was observed that the patch was tough enough to bear stretching without any damage, which could be stretched to 2.5 times its initial length (data not shown), and enough to support a weight of 100g, as shown in Fig. 2b and Fig. S1. Notably, it was found that the patch exhibited brilliant structural color and underwent a dynamic color change during the stretching. The structural color property was due to the special periodically arranged highly ordered nanostructures, which imparted the NNH patches with the property of photonic band gaps (PBGs). And light located in the PBGs at a certain wavelength is disallowed from transmitting and thus is selectively reflected, enabling the NNH patches structural colors and characteristic reflection peaks. In general, the reflection peak position of the patch could be estimated by Eq. (1):

$$\lambda = 1.633 dn_{\text{average}} \tag{1}$$

where d is the distance of the gap between diffracting planes, and $n_{\text{average}}$ is the mean refractive index of the materials. When the $n_{\text{average}}$ kept invariable, $\lambda$ would depend on interplanar distance. As the patch was
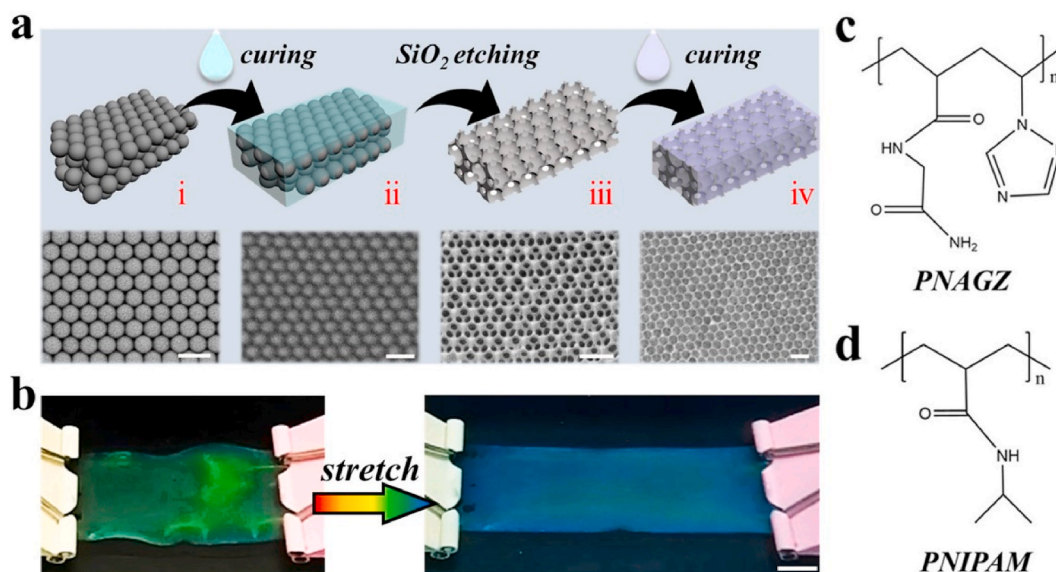
**Fig. 2.** The preparation and characterization of structured colored hydrogel patches (NNH film). a) The manufacturing processes. Schematic diagram (Top) and SEM image (Bottom) of the fabrication process. From left to right: (i) silica colloidal crystal templates (SCCs), (ii) the colloidal crystal template after the penetration of hydrogel (Hybrid film), (iii) the inverse opals, (iv) inverse opals with hydrogel filled. b) Deformations of NNH patch. The chemical structures of the c) PNAGZ and d) PNIPAM. The scale bars are 200 nm in a, and 1 cm in b.
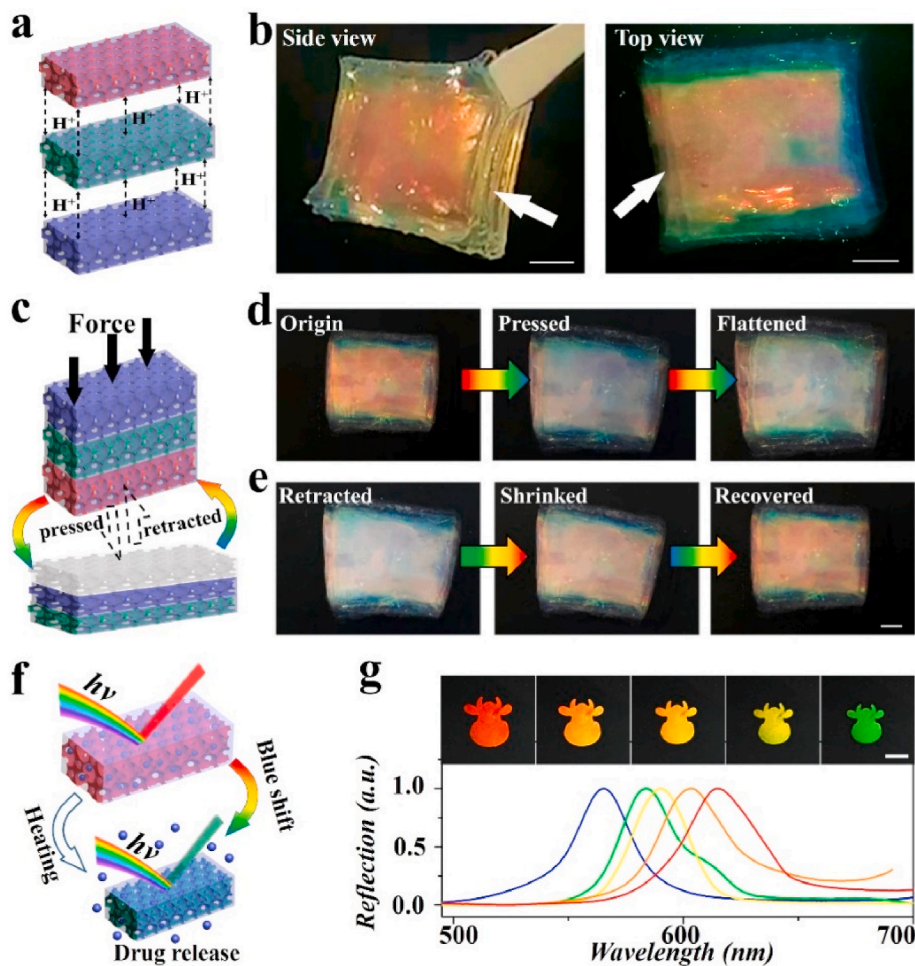


**Fig. 3.** The self-healing effect of NNH patches. a) Scheme of the self-healing mechanism of the NNH patches. b) The top and side views of the healed NNH bulk. c) Scheme of the compression of NNH bulk. Representative of d) compression and e) retraction of NNH bulk. f) Scheme of the temperature-responsive feature of the NNH patches. g) Reflection images and spectra of NNH patches at a temperature of 37 °C. The scale bars are 400 μm.

stretching, d decreased, resulting in the decrease of reflection wavelengths (Fig. S2), which exhibited that structural color of the patch was blue-shifted. Furthermore, the tensile strength tests of the PNAGZ inverse opals and NNH patches was performed (Figs. S3a and b). It was found that compared to the PNAGZ inverse opals, the strain capacity of the NNH patches was reduced due to the filling of PNIPAM hydrogels in the nanogaps of the inverse opal scaffold. On the other hand, its tensile strength was not significantly affected and was comparable to that of PNAGZ reverse opals, which was about 0.45 MPa. Further, we examined the fatigue resistance of the NNH patches stretchable properties, and found mechanical hysteresis in the patches (Fig. S3c), indicating the hydrogen bonds were sacrificed in order to dissipate the energy during the deformation process. And the sacrificial hydrogen bonds were reversible, since the hysteresis region did not show a significant decrease within 10 cycles.

Additionally, because of the presence of reversible hydrogen bonds of the PNAGZ hydrogel inverse opal scaffold, NNH patches were expected to possess self-healing capability. To verify this, multiple NNH patches with different reflection peaks were designed and stacked together, as illustrated in Fig. 3a. After placing in a sealed and constant temperature mold (40 °C) for 90 min, these stacked patches could be tightly bonded to each other, forming three-dimensional rectangular NNH bulks from the two-dimensional NNH patches, showing vibrant structural colors (Fig. 3b). To further evaluate the self-healing efficiency of patches, a compression test was performed (Fig. 3c). With the pressure-induced deformation of the hydrogel patch occurred, the multilayered structure of the hydrogel cube was revealed. And the hydrogel cube returned to its initial state when the pressure disappeared. Time and again, its structure always remained intact, demonstrating the high toughness of the inverse opal scaffolds in NNH patches. Attractively, the structural color of the patches changed with deformation. We found that, as patches were deformed, the structural color of upper patches would gradually disappear or even become transparent. Meanwhile, the structural color of the lower patches could be observed. Conversely, as patches were retracted, their structural colors could be restored (Fig. 3d and e). The structural color variations were attributed to the expansion and contraction of the nanopores under pressure. The pressure-sensing phenomenon indicated that the patches would show highly promising for sensing applications. Moreover, the compressive strengths of healed PNAGZ inverse opals and NNH patches were explored. Compared with bare PNAGZ inverse opals, the stress of NNH patches was slightly increased, whereas the strain showed the opposite trend (Fig. S4a). The phenomenon could be ascribed to the PNIPAM filler restricted the deformations of the inverse opal scaffold upon the compression. Fatigue tests on the healed NNH patches were conducted. Mechanical hysteresis in test samples was found, and the hysteresis region remained almost unchanged over 10 cycles (Fig. S4b). These results greatly demonstrated the excellent self-healing feature of the NNH patches.

Notably, taking advantage of the thermal-sensitive performance of NIPAM polymer, the patches were endowed with the ability to respond to temperature stimulation. It has been reported that the PNIPAM hydrogels would shrink in volume and release water molecules and loaded cargo, when the ambient temperature rises to its VPTT [30]. During this process, the size of the nanopores within the NNH patches would also change, leading to a variation in their PBGs, as shown in Fig. 3f. To confirm this feature, the NNH patch was placed in a simulated chronic infected wound environment, 37 °C and suitable pH [11,47], to observe the shrinkage process. To obtain suitable pH condition, the pH values of skin, normal wounds and diabetic wounds in animal models were measured. It could be indicated that diabetic wound from SD rats showed a significantly alkaline pH value, which is consistent with the reported results [47] (Fig. S5). Thus, pH 8.9 was set as the microenvironment of chronic diabetic wound. It could be found that the volume of the patch gradually shrunk, and its structural color experienced a change from red to green (Fig. 3g). This could be ascribed to the

decrease of distance between the centers of adjacent nanopores in the inverse opals. Meanwhile, reflection peaks of the patches were recorded, showing a blue-shifted trend. These results suggested the NNH patch exhibited great color-sensing property upon temperature variations, which would play an important role in monitoring the wound infection, showing the promising prospects in wound management and guidance of clinical treatment.

Besides, to investigate their ability to deliver active molecules, FITC-BSA, as a model drug for protein-like active molecules such as growth factors, was encapsulated into PNAGZ hydrogel inverse opal scaffolds. By changing PNIPAM concentrations, a series of NNH patches were fabricated, which were labeled according to the concentration of PNIPAM hydrogel. For example, NNH (5) refers to the NNH developed by integrating 5% (w/v) PNIPAM hydrogel into inverse opals. In order to investigate the effect of temperature stimulation on the release of FITC-BSA, simultaneous drug release experiments were performed under temperature stimulus and room temperature, respectively. It was found the FITC-BSA release rate of the NNH patches under temperature stimulus (37 °C) was higher than that under room temperature (25 °C), showing significant temperature sensitivity (Fig. S6a). This could be ascribed to the temperature (37 °C) exceeding the VPTT of PNIPAM hydrogels, which caused the patch to shrink and extrude the encapsulated drugs from their bodies, promoting the release of drugs. Further, the ability of different NNH patches to change dynamically in response to temperature stimuli was studied (Fig. S6c). It was found that the shift ratio of the patches gradually decreased as the concentration of PNIAPM increased. This was due to the higher the concentration of hydrogel monomers, the stronger the intermolecular forces, and the greater the resistance to temperature effects. Moreover, the NNH patches displayed repeatable and reversible reflection peak changes in many cycles, proving their good durability (Fig. S6d).

Since VTZ, as a kind of triazoles, has antibacterial, anti-spasmodic and anti-inflammatory effects [37], it was anticipated that the introduction of it could confer antibacterial and anti-inflammatory activity to the patches. To support this, *Staphylococcus aureus* (*S. aureus*) and *Escherichia coli* (*E. coli*) strains were used to examine the antibacterial activity of NNH patches. It was clearly observed that NNH patches displayed good antibacterial effectiveness against both *S. aureus* and *E. coli* from the results of scanning electron microscope (SEM) and live-dead staining (Fig. 4a and b). This could be ascribed to the presence of triazole ring nuclei, which could kill bacteria by disrupting the permeability of bacterial membranes caused by inhibiting the biosynthesis of ergosterol. In addition, since the optimal pH for most pathogenic bacteria to survive is normal to slightly alkaline (pH 7.2 to 7.6) [9], adjusting the pH of the pathogen's surroundings would be an effective strategy to enhance antibacterial activity. In practice, MES buffer was employed as a solvent to regulate pH for the preparation of NNH patches instead of double-distilled water. By this way, the patches exhibited excellent antibacterial property (about 90% against *E. coli*, and 92% against *S. aureus*) (Fig. 4c and Fig. S7). In addition, we investigated the antibacterial properties of NNH patches against *Pseudomonas aeruginosa* (PA) and *Klebsiella pneumoniae* (KP) (Fig. S8 and Table S1). It was found NNH patches have a broad-spectrum antibacterial effect. Besides, the biocompatibility of the NNH patch was further explored (Fig. S9). The cell viability of tested NNH patches exceeded 90%, indicating their low cytotoxicity. It has been demonstrated that NNH patches showed opposite effect in terms of antibacterial performance and cell biocompatibility, resulting from the presence of triazole ring nucleus, which could specifically destroy the integrity of bacterial membranes, damage the permeability of the bacterial membranes, and kill bacterium, but not damage the resident cell [37].

Given the above-mentioned outstanding features, the NNH patches were applied to treat diabetic wounds *in vivo* experiments. In detail, all diabetic rats modeled by removing some of back skin were randomly classified into five groups, and received PBS, chitosan dressings (CSD), VEGF, NNH patches, and NNH loaded VEGF (NNH-VEGF) patches,
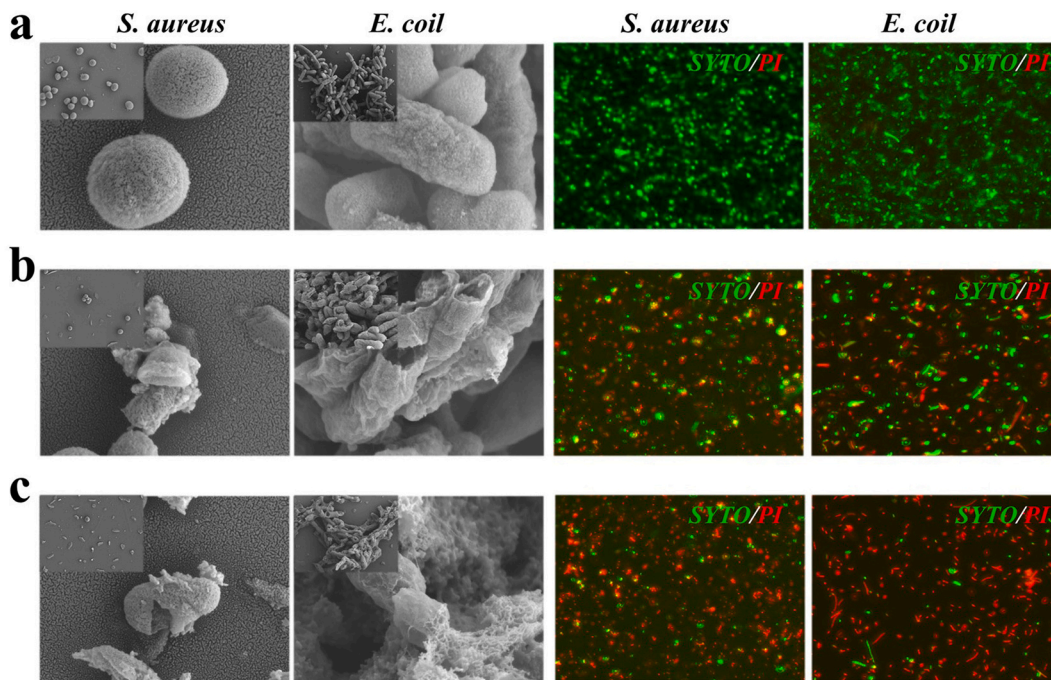
**Fig. 4.** Images of NNH patches against *S. aureus* and E. coli from scanning electron microscope (SEM) and confocal laser scanning microscopy (CLSM). a) The blank group (treated with PBS). b) NNH group (NNH patches prepared using pure water as solvent). c) NNH (MES) group (NNH patches prepared using MES buffer as solvent). The scale bars are 0.25 μm in SEM images of *S. aureus* and E. coli, 5 μm in CLSM images of *S. aureus* and *E. coli*.

respectively. Among them, PBS and CSD were recognized as negative and positive controls, respectively. The wounds of each rat showed different healing conditions (Fig. 5a). Ten days after operation, NNH-VEGF patches had the best therapeutic effect, by which the wound was almost closed. Meanwhile, the CSD treatment group showed similar results. In contrast, the PBS group had the worst wound closure. According to the quantitative results, the wound closure area in the NNH group was wider than that in the PBS group, indicating the NNH patches could promote wound healing (Fig. 5b). Notably, the wound closure was better in the NNH-VEGF group than in the NNH group, but the use of

VEGF alone was not conducive to wound closure, suggesting the NNH could improve the pathophysiological condition of the wound, thereby assisting VEGF to exert its ability. These results indicated the NNH patches had a beneficial effect on wound healing in diabetic rats, and a better effect occurred when combined with VEGF.

To further analyze the quality of wound healing, the granulation tissue formation and regenerative epithelialization by histological examination were discussed. It was found that only the wounds treated with CSD and NNH-VEGF patches showed intact new epithelium and thin thickness of granulation tissue. These regenerated epidermis and
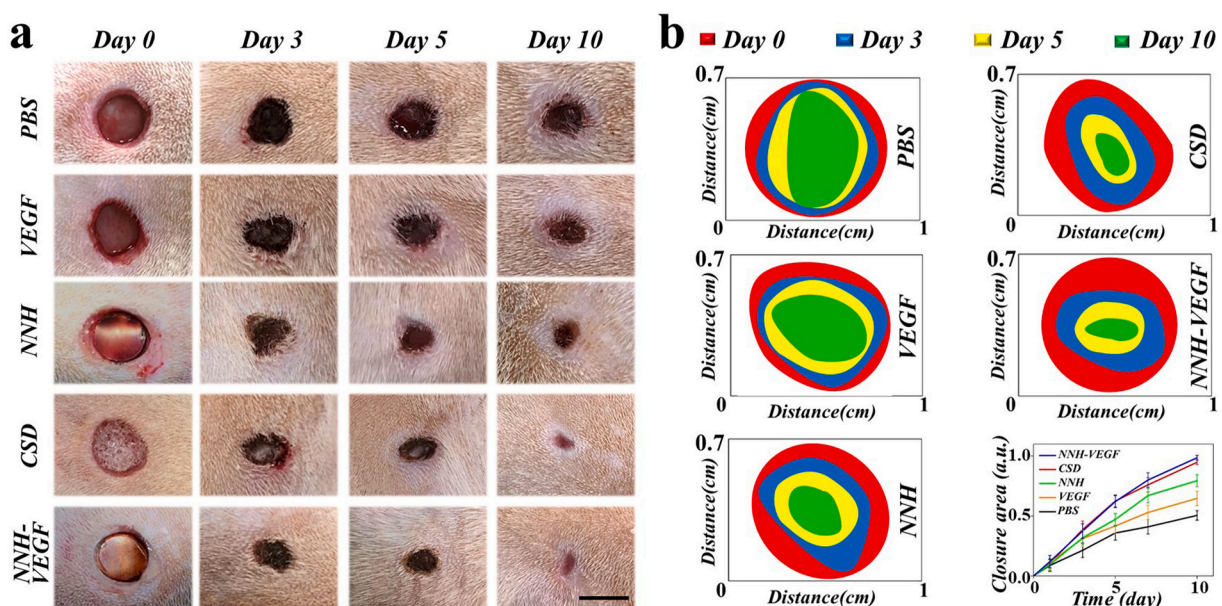


**Fig. 5.** In vivo diabetic wound healing. a) Typical images and wounds on Day 0, Day 3, Day 5, Day 10 from PBS group, VEGF group, NNH patches group, CSD group and NNH-VEGF patches group. b) The size and quantification of the wound closure area from PBS group, VEGF group, NNH patches group, CSD group and NNH-VEGF patches group. The scale bar is 7 mm.

granulation tissue, as well as the surrounding skin and subcutaneous fat, were tightly integrated, suggesting the wounds were in remodeling phase (Fig. 6a–c). Especially in the NNH-VEGF group, the wound tissue morphology was close to that of normal skin. Compared to the NNH-VEGF group, the new granulation tissue was thicker in NNH group, indicating poorer healing. In contrast, the PBS and VEGF groups had a complete absence of epidermis and exhibited markedly proliferating granulation tissue which could impede wound healing by hindering the integration of the peri-wound skin and adipose tissue. These were also illustrated by the quantitative index of the epithelial gaps in each group, as shown in Figs. S10 and S11. Collagen, which forms the matrix of the wound and stabilizes the subcutaneous connective tissue, is pivotal to the wound healing. However, in diabetic wounds, collagen deposition is impaired by the high glucose in blood, resulting in ineffective reconstruction of granulation tissue. Therefore, the quality of wound healing could also be assessed by measuring the collagen deposition in wounds. The findings showed that the collagen fibers in the NNH-VEGF group were most tightly and orderly arranged, indicating the promotion of collagen deposition. The distribution of collagen fibers in the NNH group was disorganized. In the PBS and VEGF groups, the collagen fibrils were extremely low in density and sparsely arranged (Fig. 6d). These findings illustrated that the NNH-VEGF patches could not only remodel new tissue, including new epithelium and granulation tissue, but also ameliorate the abnormalities in collagen deposition, to heal wounds.

The inflammatory phase is an essential part of promoting healing. However, in chronic wounds, such as diabetic wounds, the dysregulation of various factors, including inflammatory cytokines and growth factors, can lead to prolonged inflammatory periods and cause the non-healing wounds. Therefore, we chose these two pro-inflammatory factors IL-6 and TNF-α to assess the inflammatory response of wounds in different groups. The results of qPCR showed that the expression of mRNA of IL-6 and TNF-α in other treatments was significantly less than that in the VEGF and PBS groups. Among these treatments, the lowest expression of both IL-6 and TNF-α was detected in the NNH-VEGF group (Fig. 7a). It was worth thinking that the expression of inflammatory factors in the NNH-VEGF group was less than that in the NNH group, suggesting that the union of NNH and VEGF was more beneficial in orchestrating the inflammatory response. The same results were obtained for immunohistochemical detection and quantitative analysis of IL-6 and TNF-α, demonstrating the NNH-VEGF patches could effectively regulate the process of diabetic wound healing through anti-inflammation and delivery of VEGF (Fig. S12). Barren angiogenesis and impaired microcirculation are also responsible for non-healing diabetic wounds. Thus, the immunofluorescence co-staining for CD31 and α-SMA was employed to detect angiogenesis in the wound tissues. Like the previous elaborated results, the maximum area of angiogenesis was generated in the NNH-VEGF group, followed by the CSD, NNH, VEGF, and PBS groups (Fig. 7b). Notably, the use of VEGF alone did not have a promotion on angiogenesis compared to the NNH-VEGF group that also utilized VEGF (Fig. S12). The reason for this may be the alkaline microenvironment with a wound pH up to 8.9 triggered by long-term inflammation resulted in compromised activity or even inactivation of proteins. However, in the NNH-VEGF group, the NNH patches could regulate the pH of the wound microenvironment by attenuating inflammation on account of the downregulation of inflammatory factor expression, thereby increasing the activity of released VEGF. This does strongly support an effective strategy to develop active dressings by combining NNH patches with active molecules for wound healing.

## 4. Conclusion

In this work, we have engineered and demonstrated a responsive and self-healing structural color hydrogel patch to enhance wound healing and skin tissue regeneration in diabetic chronic wounds. Due to the combination of the functional hydrogels with the inverse opal scaffold, the prepared hydrogel patch has good mechanical strength and self-
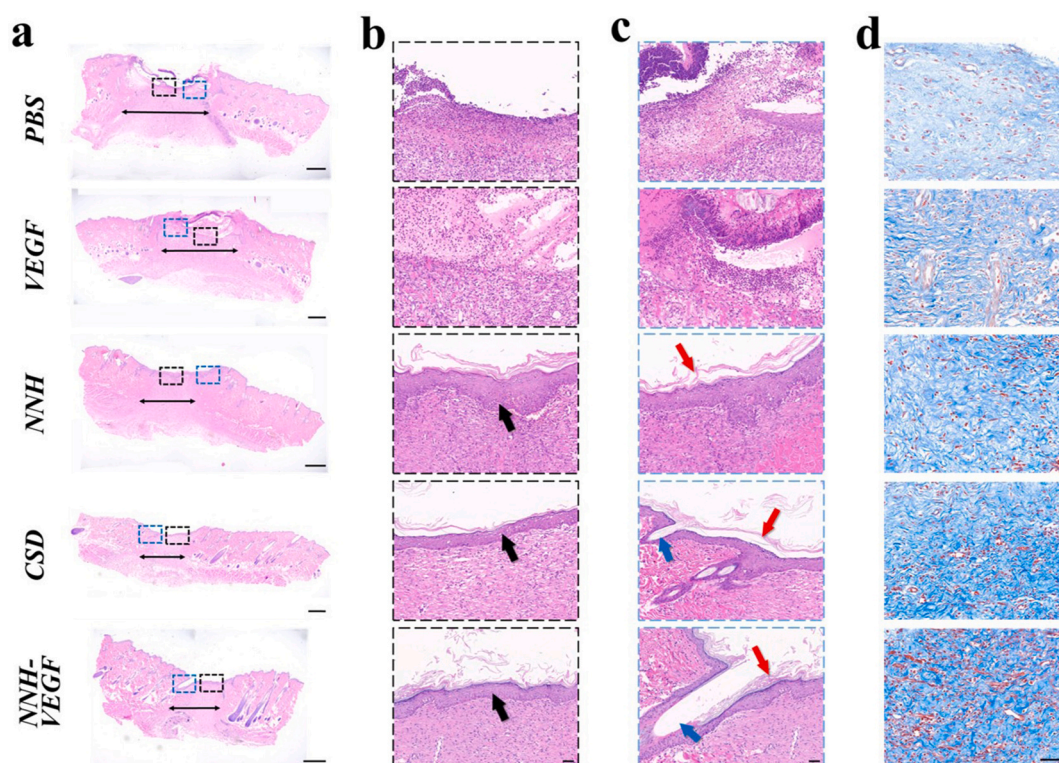


**Fig. 6.** Hematoxylin and eosin staining of sections from each group after 10 days. a) The overall structure of the skin tissue. b) Epithelial regeneration in the wound indicated by black arrows. c) Remodeling at the wound margin indicated by red arrows, and hair follicle indicated by blue arrows. d) Collagen deposition in the wound tissue. The scale bars are 500 μm in a, 50 μm in b, c and d.
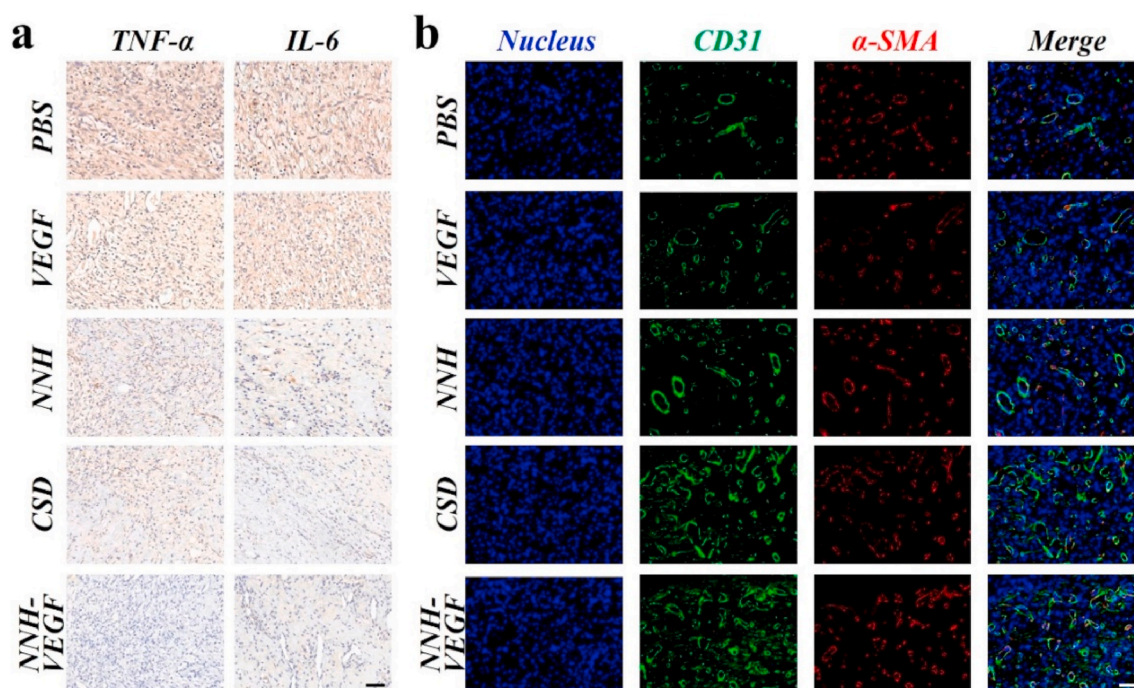
**Fig. 7.** Immunostaining for (a) TNF-α and IL-6 and immunofluorescence staining for (b) CD31 and α-SMA of sections from each group after 10 days. The scale bars are 50 μm.

healing ability, which prevents local stress damage and further facilitates its practical application. In addition, the introduction of PNIPAM hydrogel imparts the hydrogel patch with temperature response performance. With the merits of the presence of inverse opal structures, the hydrogel patch exhibits color-sensing property in response to temperature variations, which can be applied for monitoring wound infection, realizing effective wound management, and guiding clinical treatment. Importantly, the hydrogel patch, also has a variety of biological activities such as antibacterial, anti-inflammatory, and pro-angiogenic, enabling significant wound healing in chronic diabetic wounds. All of these indicate the hydrogel patches have a promising, practical potential in the effective management of chronic wounds in diabetes.

Despite these outstanding functionalities, including superior mechanical properties, self-healing, antibacterial properties, thermal-responsiveness performance, color-sensing behavior as well as wound repair capability, challenges remain and efforts must be devoted for a wider range of practical applications. As reported that pressure therapy has been used to promote the healing of burn wounds, it is anticipated that applying pressure on diabetic wounds through the patches would be an effective way to promote diabetic wound healing. Besides, considering the previous researches that adopted an electrochemical-based approach for monitoring of wound infection, the concept for visual monitoring wound infection *in vivo* based on structural color variations of the patches could be achieved through further optimizing the materials and measurement approaches.

## CRediT authorship contribution statement

**Canwen Chen:** Validation, Formal analysis, Investigation, Data curation, Writing – original draft. **Yu Wang:** Resources, Writing – review & editing. **Han Zhang:** Writing – review & editing. **Hui Zhang:** Writing – review & editing. **Weiliang Dong:** Conceptualization, Methodology, Supervision. **Weijian Sun:** Conceptualization, Methodology, Supervision. **Yuanjin Zhao:** Conceptualization, Methodology, Supervision.

## Declaration of competing interest

The authors declare that they have no known competing financial interests or personal relationships that could have appeared to influence the work reported in this paper.

## Appendix A. Supplementary data

Supplementary data to this article can be found online at https://doi.org/10.1016/j.bioactmat.2021.11.037.

## References

[1] E.J. Williamson, A.J. Walker, K. Bhaskaran, S. Bacon, C. Bates, C.E. Morton, H. J. Curtis, A. Mehrkar, D. Evans, P. Inglesby, J. Cockburn, H.I. McDonald, B. MacKenna, L. Tomlinson, I.J. Douglas, C.T. Rentsch, R. Mathur, A.Y.S. Wong, R. Grieve, D. Harrison, H. Forbes, A. Schultze, R. Croker, J. Parry, F. Hester, S. Harper, R. Perera, S.J.W. Evans, L. Smeeth, G. Ben, Factors associated with COVID-19-related death using OpenSAFELY, Nature 584 (7821) (2020) 430–436.
[2] G. Mingrone, S. Panunzi, A. De Gaetano, C. Guidone, A. Iaconelli, E. Capristo, G. Chamseddine, S.R. Bornstein, F. Rubino, Metabolic surgery versus conventional medical therapy in patients with type 2 diabetes: 10-year follow-up of an open-label, single-centre, randomised controlled trial, Lancet 397 (10271) (2021) 293–304.
[3] K.S. Ruth, F.R. Day, J. Tyrrell, D.J. Thompson, A.R. Wood, A. Mahajan, R. N. Beaumont, L. Wittemans, S. Martin, A.S. Busch, A.M. Erzurumluoglu, B. Hollis, T.A. O'Mara, M.I. McCarthy, C. Langenberg, D.F. Easton, N.J. Wareham, S. Burgess, A. Murray, K.K. Ong, T.M. Frayling, J.R. B Perry, Using human genetics to understand the disease impacts of testosterone in men and women, Nat. Med. 26 (2) (2020) 252–258.
[4] B. Yu, C.Z. Li, Y. Sun, D.W. Wang, Insulin treatment is associated with increased mortality in patients with COVID-19 and type 2 diabetes, Cell Metabol. 33 (1) (2021) 65–77.
[5] M. Costa-Mattioli, P. Walter, The integrated stress response: from mechanism to disease, Science 368 (6489) (2020) eaat5314.

[6] C.G. Schalkwijk, C.D. A Stehouwer, Methylglyoxal, a highly reactive dicarbonyl compound, in diabetes, its vascular complications, and other age-related diseases, Physiol. Rev. 100 (1) (2020) 407–461.

[7] S.A. Eming, T.A. Wynn, P. Martin, Inflammation and metabolism in tissue repair and regeneration, Science 356 (6342) (2017) 1026–1030.

[8] M.A. Atkinson, G.S. Eisenbarth, A.W. Michels, Type 1 diabetes, Lancet 383 (9911) (2014) 69–82.

[9] Z.R. Jia, J.L. Gong, Y. Zeng, J.H. Ran, J. Liu, K.F. Wang, C.M. Xie, X. Lu, J. Wang, Bioinspired conductive silk microfiber integrated bioelectronic for diagnosis and wound healing in diabetes, Adv. Funct. Mater. 31 (19) (2021), 2010461.

[10] L.Y. Sun, L. Fan, F.K. Bian, G.P. Chen, Y.T. Wang, Y.J. Zhao, MXene-integrated microneedle patches with innate molecule encapsulation for wound healing, Research (2021), 9838490, 2021.

[11] Y.N. Zhu, J.M. Zhang, J.Y. Song, J. Yang, Z. Du, W.Q. Zhao, H.S. Guo, C.Y. Wen, Q. S. Li, X.J. Sui, L. Zhang, A multifunctional pro-healing Zwitterionic hydrogel for simultaneous optical monitoring of pH and glucose in diabetic wound treatment, Adv. Funct. Mater. 30 (6) (2020), 1905493.

[12] Y.S. Zhang, K. Yue, J. Aleman, K. Mollazadeh-Moghaddam, S.M. Bakht, J.Z. Yang, W.T. Jia, V. Dell'Erba, P. Assawes, S.R. Shin, M.R. Dokmeci, R. Oklu, A. Khademhosseini, 3D bioprinting for tissue and organ fabrication, Ann. Biomed. Eng. 45 (1) (2017) 148–163.

[13] Y. Zaokari, A. Persaud, A. Ibrahim, Biomaterials for adhesion in orthopedic applications: a review, Engineered Regeneration 1 (2020) 51–63.

[14] G.P. Chen, Y.R. Yu, G.F. Wang, G.S. Gu, X.W. Wu, J.A. Ren, H.D. Zhang, Y.J. Zhao, Microfluidic electrospray vitamin metal-organic frameworks encapsulated microcapsules for wound healing, Research (2019), 6175398, 2019.

[15] A.K. Miri, I. Mirzaee, S. Hassan, S.M. Oskui, D. Nieto, A. Khademhosseini, Y. S. Zhang, Effective bioprinting resolution in tissue model fabrication, Lab Chip 19 (11) (2019) 2019–2037.

[16] Y.Z. Zhang, J. Tu, D.Q. Wang, H.T. Zhu, S.K. Maity, X.M. Qu, B. Bogaert, H. Pei, H. B. Zhang, Programmable and multifunctional DNA-based materials for biomedical applications, Adv. Mater. 30 (24) (2018), 1703658.

[17] C.W. See, T. Kim, D.H. Zhu, Hernia mesh and hernia repair: a review, Engineered Regeneration 1 (2020) 19–33.

[18] S. Shi, M.A. Cui, F.X. Sun, K.K. Zhu, M.I. Iqbal, X.Y. Chen, B. Fei, R.K.Y. Li, Q. Y. Xia, J.L. Hu, An innovative solvent-responsive coiling–expanding stent, Adv. Mater. (2021) 2101005.

[19] J.H. He, Z.X. Zhang, Y.T. Yang, F.G. Ren, J.P. Li, S.J. Zhu, F. Ma, R.Q. Wu, Y. Lv, G. He, B.L. Guo, D. Chu, Injectable self-healing adhesive pH-responsive hydrogels accelerate gastric hemostasis and wound healing, Nano-Micro Lett. 13 (1) (2021) 80.

[20] M. Safonov, J. You, J.Y. Lee, V.L. Safonov, D. Berman, D.H. Zhu, Hydrogen generating patch improves skin cell viability, migration activity, and collagen expression, Engineered Regeneration 1 (2020) 1–5.

[21] S. Park, S.S. Lee, S.H. Kim, Photonic multishells composed of cholesteric liquid crystals designed by controlled phase separation in emulsion drops, Adv. Mater. 32 (30) (2020), 2002166.

[22] Z.K. Gu, Z.D. Huang, X.T. Hu, Y. Wang, L.H. Li, M.Z. Li, Y.L. Song, In situ inkjet printing of the perovskite single-crystal array-embedded polydimethylsiloxane film for wearable light-emitting devices, ACS Appl. Mater. Interfaces 12 (19) (2020) 22157–22162.

[23] S.C. Qi, P.F. Zhang, M. Ma, M.H. Yao, J.J. Wu, E. Makila, J. Salonen, H. Ruskoaho, Y.Z. Xu, H.A. Santos, H.B. Zhang, Cellular internalization-induced aggregation of porous silicon nanoparticles for ultrasound imaging and protein-mediated protection of stem cells, Small 15 (1) (2019), 1804332.

[24] M.A. Wang, W.L. Li, G.S. Tang, C.E. Garciamendez-Mijares, Y.S. Zhang, Engineering (Bio)Materials through shrinkage and expansion, Adv. Healthc. Mater. 10 (14) (2021) 2100380.

[25] M.T. Hua, D. Wu, S.W. Wu, Y.F. Ma, Y. Alsaid, X.M. He, 4D printable tough and thermoresponsive hydrogels, ACS Appl. Mater. Interfaces 13 (11) (2021) 12689–12697.

[26] Y.H. Wang, L. Lu, G.X. Zheng, X.C. Zhang, Microenvironment-controlled micropatterned microfluidic model (MMMM) for biomimetic in situ studies, ACS Nano 14 (8) (2020) 9861–9872.

[27] Y.C. Guo, Y. Wang, X.H. Zhao, X. Li, Q. Wang, W. Zhong, K. Mequanint, R.X. Zhan, M. Xing, G.X. Luo, Snake extract–laden hemostatic bioadhesive gel cross-linked by visible light, Sci. Adv. 7 (29) (2021), eabf9635.

[28] D.L. Cao, X. Chen, F. Cao, W. Guo, J.Y. Tang, C.Y. Cai, S.Q. Cui, X.W. Yang, L. Yu, Y. Su, J.D. Ding, An intelligent transdermal formulation of ALA-loaded copolymer thermogel with spontaneous asymmetry by using temperature-induced sol-gel transition and gel-sol (suspension) transition on different sides, Adv. Funct. Mater. 31 (22) (2021), 2100349.

[29] L. Saunders, P.X. Ma, Self-healing supramolecular hydrogels for tissue engineering applications, Macromol. Biosci. 19 (1) (2019), 1800313.

[30] X.H. Zhao, X.Y. Chen, H. Yuk, S.T. Lin, X.Y. Liu, G. Parada, Soft materials by design: unconventional polymer networks give extreme properties, Chem. Rev. 121 (8) (2021) 4309–4372.

[31] X.S. Qian, Y.S. Zhao, Y. Alsaid, X. Wang, M.T. Hua, T. Galy, H. Gopalakrishna, Y. Y. Yang, J.S. Cui, N. Liu, M. Marszewski, L. Pilon, H.Q. Jiang, X.M. He, Artificial phototropism for omnidirectional tracking and harvesting of light, Nat. Nanotechnol. 14 (11) (2019) 1048–1055.

[32] L. Siebert, E. Luna-Ceron, L.E. Garcia-Rivera, J. Oh, J. Jang, D.A. Rosas-Gomez, M. D. Perez-Gomez, G. Maschkowitz, H. Fickenscher, D. Oceguera-Cuevas, C. G. Holguin-Leon, B. Byambaa, M.A. Hussain, E. Enciso-Martinez, M. Cho, Y. Lee, N. Sobahi, A. Hasan, D.P. Orgill, Y.K. Mishra, R. Adelung, E. Lee, S.R. Shin, Light-controlled growth factors release on tetrapodal ZnO-incorporated 3D-printed hydrogels for developing smart wound scaffold, Adv. Funct. Mater. 31 (22) (2021), 2007555.

[33] D.J. Kim, J. Yoon, D.H. Kim, S.G. Park, S.H. Kim, Plasmonic microgels for Raman-based molecular detection created by simultaneous photoreduction and photocross-linking, ACS Appl. Mater. Interfaces 12 (42) (2020) 48188–48197.

[34] C.Y. Jiang, L.Z. Zhang, Q. Yang, S.X. Huang, H.P. Shi, Q. Long, B. Qian, Z.H. Liu, Q. B. Guan, M.J. Liu, R.H. Yang, Q. Zhao, Z.W. You, X.F. Ye, Self-healing polyurethane-elastomer with mechanical tunability for multiple biomedical applications *in vivo*, Nat. Commun. 12 (1) (2021) 4395.

[35] C. Ma, J. Sun, B. Li, Y. Feng, Y. Sun, L. Xiang, B.H. Wu, L.L. Xiao, B.M. Liu, V. S. Petrovskii, L. Bin, J.R. Zhang, Z.L. Wang, H.Y. Li, L. Zhang, J.J. Li, F. Wang, R. Göstl, I. I Potemkin, D. Chen, H.B. Zeng, H.J. Zhang, K. Liu, A. Herrmann, Ultra-strong bio-glue from genetically engineered polypeptides, Nat. Commun. 12 (1) (2021) 3613.

[36] J. Sun, L.L. Xiao, B. Li, K.L. Zhao, Z.L. Wang, Y. Zhou, C. Ma, J.J. Li, H.J. Zhang, A. Herrmann, K. Liu, Genetically engineered polypeptide adhesive coacervates for surgical applications, Angew. Chem. Int. Ed. (2021), https://doi.org/10.1002/anie.202100064.

[37] H.B. Wang, H. Zhu, W.G. Fu, Y.Y. Zhang, B. Xu, F. Gao, Z.Q. Cao, W.G. Liu, A high strength self-healable antibacterial and anti-inflammatory supramolecular polymer hydrogel, Macromol. Rapid Commun. 38 (9) (2017), 1600695.

[38] M. Zhang, H. Zhang, M. He, L.H. Wang, H.J. Yang, Y.L. Song, Controlled diffusion of nanoparticles by viscosity gradient for photonic crystal with dual photonic band gaps, Nanotechnology 31 (43) (2020), 435604.

[39] C.M. Shao, Y.X. Liu, J.J. Chi, J. Wang, Z. Zhao, Y.J. Zhao, Photo-controllable inverse opal graphene hydrogel scaffolds with biomimetic enrichment capability for cell culture, Research (2019), 9783793, 2019.

[40] S.K. Nam, J.B. Kim, S.H. Han, S.H. Kim, Photonic janus balls with controlled magnetic moment and density asymmetry, ACS Nano 14 (11) (2020) 15714–15722.

[41] L. Wu, Z.C. Dong, Z.R. Cai, T. Ganapathy, N.X. Fang, C.X. Li, C.L. Yu, Y. Zhang, Y. L. Song, Highly efficient three-dimensional solar evaporator for high salinity desalination by localized crystallization, Nat. Commun. 11 (1) (2020) 521.

[42] Z.M. Tang, X.C. Zhang, Y.Q. Shu, M. Guo, H. Zhang, W. Tao, Insights from nanotechnology in COVID-19 treatment, Nano Today 36 (2021), 101019.

[43] H.J. Sun, N. Gao, K. Dong, J.S. Ren, X.G. Qu, Graphene quantum dots-band-aids used for wound disinfection, ACS Nano 8 (6) (2014) 6202.

[44] J.J. Mendes, C.I. Leandro, D.P. Bonaparte, A.L. Pinto, A rat model of diabetic wound infection for the evaluation of topical antimicrobial therapies, Comp. Med. 62 (1) (2012) 37.

[45] S.V.B. Singh, H. Park, G. Khang, D. Lee, Hydrogen peroxide-responsive engineered polyoxalate nanoparticles for enhanced wound healing, Macromol. Res. 26 (1) (2018) 40.

[46] P.B. Milan, N. Lotfibakhshaiesh, M.T. Joghataie, J. Ai, A. Pazouki, D.L. Kaplan, S. Kargozar, N. Amini, M.R. Hamblin, M. Mozafari, A. Samadikuchaksaraei, Accelerated wound healing in a diabetic rat model using decellularized dermal matrix and human umbilical cord perivascular cells, Acta Biomater. 45 (2016) 234.

[47] A. McLister, J. McHugh, J. Cundell, J. Davis, New developments in smart bandage technologies for wound diagnostics, Adv. Mater. 28 (27) (2016) 5732.